

Structure and magnetism of $(\text{La}/\text{Sr})_2\text{M}_{0.5}\text{Ir}^{\text{V}}_{0.5}\text{O}_4$ and topochemically reduced $(\text{La}/\text{Sr})_2\text{M}_{0.5}\text{Ir}^{\text{II}}_{0.5}\text{O}_3$ ($\text{M} = \text{Fe}, \text{Co}$) complex oxides.

Jacob E. Page[†] and Michael A. Hayward^{*}

Department of Chemistry, University of Oxford, Inorganic Chemistry Laboratory, South Parks Road, Oxford, OX1 3QR, U.K.

Supporting Information Placeholder

ABSTRACT: Neutron powder diffraction data show that $\text{Sr}_2\text{Fe}_{0.5}\text{Ir}_{0.5}\text{O}_4$, $\text{Sr}_2\text{Co}_{0.5}\text{Ir}_{0.5}\text{O}_4$ and $\text{La}_{0.5}\text{Sr}_{1.5}\text{Co}_{0.5}\text{Ir}_{0.5}\text{O}_4$ all adopt undistorted, $n = 1$ Ruddlesden-Popper structures in which the Ir^{5+} and $\text{Fe}^{3+}/\text{Co}^{3+}/\text{Co}^{2+}$ cations are statistically disordered over all the octahedral coordination sites. Magnetization data indicate the two cobalt phases are spin-glasses at low temperature while $\text{Sr}_2\text{Fe}_{0.5}\text{Ir}_{0.5}\text{O}_4$ appears to adopt an antiferromagnetic state with very small magnetically ordered domains. Topochemical reduction with a Zr getter converts the tetragonal $\text{A}_2\text{M}_{0.5}\text{Ir}_{0.5}\text{O}_4$ phases to the corresponding orthorhombic $\text{A}_2\text{M}_{0.5}\text{Ir}_{0.5}\text{O}_3$ phases in which the Ir^{2+} and $\text{Fe}^{2+}/\text{Co}^{2+}/\text{Co}^{1+}$ cations are located in approximately square-planar coordination sites. Magnetization data indicate $\text{Sr}_2\text{Fe}_{0.5}\text{Ir}_{0.5}\text{O}_3$ is a spin-glass below $T_G \sim 30$ K, while $\text{Sr}_2\text{Co}_{0.5}\text{Ir}_{0.5}\text{O}_3$ appears to be antiferromagnetic below $T_N \sim 25$ K and $\text{La}_{0.5}\text{Sr}_{1.5}\text{Co}_{0.5}\text{Ir}_{0.5}\text{O}_3$ shows no sign of magnetic order for $T > 5$ K. The magnetic behavior of both the $\text{A}_2\text{M}_{0.5}\text{Ir}_{0.5}\text{O}_4$ and $\text{A}_2\text{M}_{0.5}\text{Ir}_{0.5}\text{O}_3$ phases is discussed on the basis of metal d-electron count and structural features.

Introduction

Complex oxides containing 5d transition metals have attracted a lot of attention recently because strong spin-orbit coupling (SOC) can lead to these ions adopting local electronic configurations which are qualitatively different from lighter 3d and 4d analogues.¹ Taking iridium as an example it is observed that in many cases the SOC interactions are of comparable magnitude to crystal field effects (Δ). As a consequence the d-states of an octahedrally coordinated iridium cation are first split into the familiar t_{2g} and e_g sets by the crystal field, with the t_{2g} set further split into a quartet $J = 3/2$ state and a doublet $J = 1/2$ state by the strong SOC interactions. The energy separation between the $J = 3/2$ and $J = 1/2$ states can be many times kT at room temperature, so the $5d^4$ electron count of Ir^{5+} leads to a complete occupation of the $J = 3/2$ state/band and the expectation of diamagnetic behavior – a situation in strong contrast to $3d^4$ and $4d^4$ systems. Indeed many Ir^{5+}O_6 systems are observed to have small magnetic moments, although there is a growing body of evidence that under the appropriate conditions Ir^{5+} centers can exhibit small finite moments and even magnetically ordered states.²⁻⁵

Systems containing Ir^{4+}O_6 units have also been extensively studied.⁶⁻⁸ In this case the $5d^5$ configuration of Ir^{4+} completely fills the $J = 3/2$ state/band and half-fills the $J = 1/2$ state/band. This latter partially filled band can be sufficiently narrow that the modest on-site repulsion energies (U) of the 5d orbitals can be sufficient to open a Mott gap, leading to antiferromagnetic insulating

behavior in phases such as Sr_2IrO_4 .⁹ Thus we can see that the combination of strong SOC, ligand-field and on-site coulombic repulsion can lead to insulating phases – a situation apparently at odds with the simple expectation that the radially extended 5d orbitals will yield wide d-orbital based bands and itinerant electron behavior.

Recently we have been trying to extend the scope of iridium oxide chemistry by preparing novel phases contain iridium cations in low oxidation states, *via* topochemical reduction. This led to the formation of the first Ir^{2+} -containing complex oxide $\text{Sr}_2\text{FeIrO}_4$, *via* the reduction of the double perovskite $\text{Sr}_2\text{FeIrO}_6$.¹⁰ $\text{Sr}_2\text{FeIrO}_4$ exhibits complex magnetic behavior in which the nearest neighbor Fe-Ir and Ir-Ir couplings are frustrated – a situation which is ultimately resolved when a large magnetostrictive distortion lifts the frustration in the system. Both the Fe^{2+} and Ir^{2+} cations within $\text{Sr}_2\text{FeIrO}_4$ occupy square-planar coordination sites and during the analysis of the complex behavior of the phase we observed a strong analogy between the local electronic states of square-planar Ir^{2+} and octahedrally coordinated Ir^{4+} as both systems have 5 electrons distributed over a near-degenerate $d_{xz}/d_{yz}/d_{xy}$ orbital triplet as shown schematically in Figure 1. Support for this analogy is also provided by observing the density of states close to the Fermi level of $\text{Sr}_2\text{FeIrO}_4$ and $\text{La}_2\text{ZnIrO}_6$ are very similar – the only exception being the $\text{Sr}_2\text{FeIrO}_4$ has a filled Ir d_{z^2} band below the Fermi level while the corresponding band in $\text{La}_2\text{ZnIrO}_6$ is empty and lies well above the Fermi level.¹⁰⁻¹¹

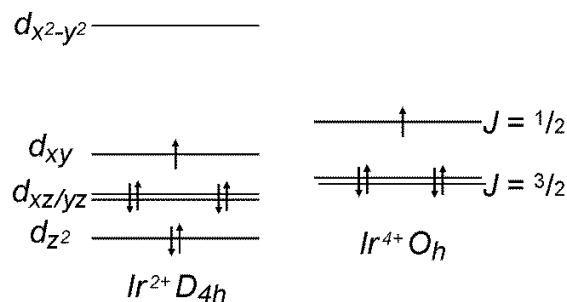


Figure 1. Schematic diagram illustrating the analogy between the orbital/state energies of square-planar Ir^{2+}O_4 and octahedral Ir^{4+}O_6 .

The analogy between square-planar Ir^{2+} and octahedral Ir^{4+} has motivated us to investigate further Ir^{2+} -containing oxides. To that end we have prepared the Ir^{5+} -containing Ruddlesden-Popper phases $\text{Sr}_2\text{Fe}_{0.5}\text{Ir}_{0.5}\text{O}_4$, $\text{Sr}_2\text{Co}_{0.5}\text{Ir}_{0.5}\text{O}_4$ ¹²⁻¹⁵ and $\text{La}_{0.5}\text{Sr}_{1.5}\text{Co}_{0.5}\text{Ir}_{0.5}\text{O}_4$ and then reduced them to the corresponding

$A_2M_{0.5}Ir_{0.5}O_3$ Ir^{2+} compounds to study the effect of strong SOC on the magnetic behavior both the Ir^{5+} and Ir^{2+} systems.

Experimental

Synthesis of $A_2M_{0.5}Ir_{0.5}O_4$. Samples of $Sr_2Fe_{0.5}Ir_{0.5}O_4$, $Sr_2Co_{0.5}Ir_{0.5}O_4$ and $La_{0.5}Sr_{1.5}Co_{0.5}Ir_{0.5}O_4$ were prepared using a citrate gel method.⁵ Appropriate quantities of $SrCO_3$ (99.994%), La_2O_3 (99.999%, dried at 900 °C) and Fe (99.99%) or Co (99.996%) were dissolved in a 1:1 mixture of concentrated nitric acid and distilled water, then the required amount of IrO_2 (99.99%, dried at 700 °C for 2 hours) was added. Citric acid and analar ethylene glycol were added and the solutions were heated whilst being stirred. The gels thus formed were allowed to combust in air and the subsequent products were ground into fine powders, placed in alumina crucibles and then heated in air, at a rate of 1 °C min⁻¹ to 1000 °C, to remove the remaining organic components from the samples. The samples were then pressed into pellets and $Sr_2Fe_{0.5}Ir_{0.5}O_4$ and $Sr_2Co_{0.5}Ir_{0.5}O_4$ were heated in air for two periods of 2d at 1000 °C with the $Sr_2Fe_{0.5}Ir_{0.5}O_4$ samples heated for a further 2d at 1100 °C. Samples of $La_{0.5}Sr_{1.5}Co_{0.5}Ir_{0.5}O_4$ were heated at 1300 °C for two periods of 2d.

Topochemical reduction of $A_2M_{0.5}Ir_{0.5}O_4$ phases. Samples of $Sr_2Fe_{0.5}Ir_{0.5}O_4$, $Sr_2Co_{0.5}Ir_{0.5}O_4$ and $La_{0.5}Sr_{1.5}Co_{0.5}Ir_{0.5}O_4$ were reduced using a zirconium getter. Samples to be reduced were sealed in an evacuated silica ampoule along with a glass ‘thimble’ containing powdered zirconium such that the two powders shared an atmosphere but were not in physical contact. This apparatus was then heated for multiple periods with the sample being re-ground, and the Zr powder being replaced with unreacted material between heating periods. Samples of $Sr_2Fe_{0.5}Ir_{0.5}O_{4-x}$ were prepared by heating for 3 periods of 7d at 410 °C; Samples of $Sr_2Co_{0.5}Ir_{0.5}O_{4-x}$ were prepared by heating for 5 periods of 7d at 320 °C; samples of $La_{0.5}Sr_{1.5}Co_{0.5}Ir_{0.5}O_{4-x}$ were prepared by heating for 10 periods of 7d at 550 °C.

Characterization. X-ray powder diffraction data were collected from samples contained in gas-tight sample holders using a PANalytical X’Pert diffractometer incorporating an X’celerator position sensitive detector (monochromatic Cu K α 1 radiation). Neutron powder diffraction data were collected using the D2b instrument (ILL neutron source, France) from samples contained within vanadium cans sealed under argon. Rietveld profile refinements were performed using the GSAS suite of programs.¹⁶ DC and AC magnetization data were collected using a Quantum Design MPMS SQUID magnetometer. Thermogravimetric measurements were performed by heating powder samples at a rate of 5 °C min⁻¹ under a flowing oxygen atmosphere, using a Mettler-Toledo MX1 thermogravimetric microbalance.

Results

Structural characterization of $A_2M_{0.5}Ir_{0.5}O_4$ phases. Neutron powder diffraction data collected from $Sr_2Fe_{0.5}Ir_{0.5}O_4$, $Sr_2Co_{0.5}Ir_{0.5}O_4$ and $La_{0.5}Sr_{1.5}Co_{0.5}Ir_{0.5}O_4$ at room temperature could be readily indexed on the basis of body-centered tetragonal unit cells consistent with the formation of $n = 1$ Ruddlesden-Popper phases, as has been previously reported for $Sr_2Co_{0.5}Ir_{0.5}O_4$.¹² Structural models were constructed based on the reported structure of $Sr_2Co_{0.5}Ir_{0.5}O_4$, with appropriate Fe/Ir or Co/Ir solid solution on the B-site and a 1:3 La:Sr solid solution on the A-site of the $La_{0.5}Sr_{1.5}Co_{0.5}Ir_{0.5}O_4$ model. These models were refined against the neutron diffraction data. In all the refinements all atomic positional parameters were refined as were anisotropic atomic displacement parameters for all atoms.

All three refinements converged readily to give good fits to the data and they revealed no indication of secondary phases in any of the samples. Full details of the refined structures of $Sr_2Fe_{0.5}Ir_{0.5}O_4$, $Sr_2Co_{0.5}Ir_{0.5}O_4$ and $La_{0.5}Sr_{1.5}Co_{0.5}Ir_{0.5}O_4$ are given in Tables S1, S2

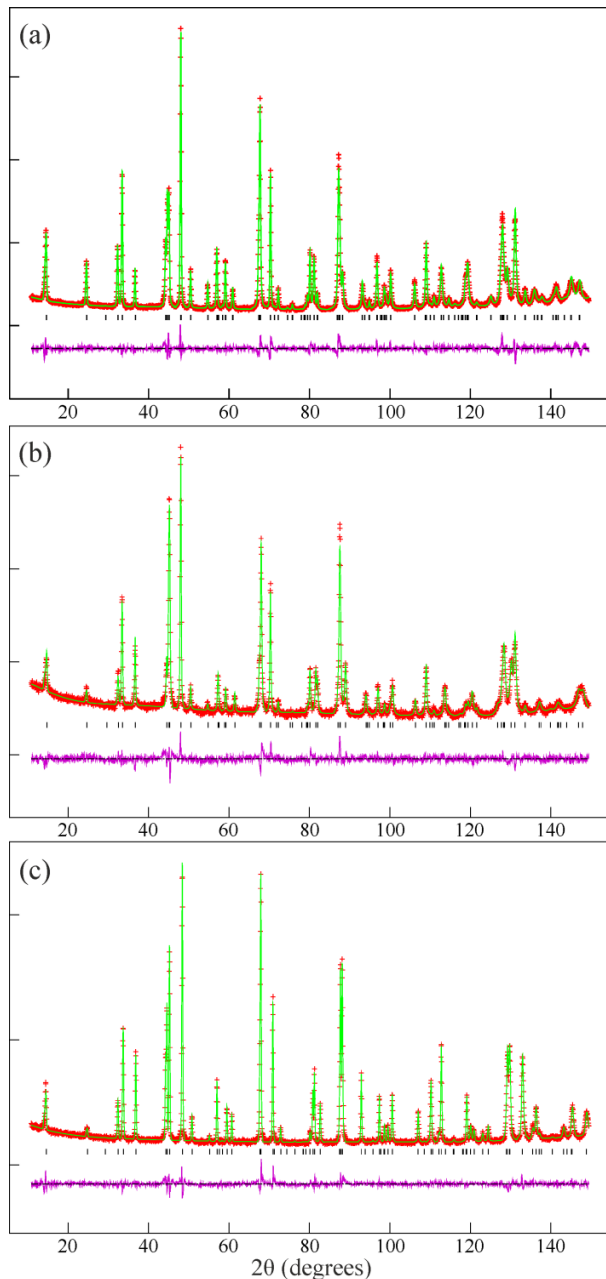


Figure 2. Observed, calculated and difference plots from the structural refinement of a) $Sr_2Fe_{0.5}Ir_{0.5}O_4$, b) $Sr_2Co_{0.5}Ir_{0.5}O_4$ and c) $La_{0.5}Sr_{1.5}Co_{0.5}Ir_{0.5}O_4$ against neutron powder diffraction data collected at 298 K.

and S3 respectively in the Supporting Information with plots of the observed and calculated data shown in Figures 2a, 2b and 2c respectively and selected bond lengths are listed in Table 1. The structure refined for $Sr_2Co_{0.5}Ir_{0.5}O_4$ is in good agreement with previous reports.¹²

Magnetic characterization of $Sr_2Fe_{0.5}Ir_{0.5}O_4$. DC zero-field cooled (ZFC) and field cooled (FC) magnetization data collected from $Sr_2Fe_{0.5}Ir_{0.5}O_4$ as a function of temperature, in an applied field of 100 Oe, are shown in Figure 3. On cooling the ZFC and FC data diverge weakly below $T \sim 170$ K, before both data sets undergo an anomaly at $T \sim 50$ K and diverge more strongly. The ZFC and FC data do not obey the Curie-Weiss law over any significant temperature range. Field dependent data collected at 300 K and 100 K, shown in the inset to Figure 3, are linear and pass

Cation	Anion	$\text{Sr}_2\text{Fe}_{0.5}\text{Ir}_{0.5}\text{O}_4$	$\text{Sr}_2\text{Co}_{0.5}\text{Ir}_{0.5}\text{O}_4$	$\text{La}_{0.5}\text{Sr}_{1.5}\text{Co}_{0.5}\text{Ir}_{0.5}\text{O}_4$
Sr/La	O(1) \times 1	2.440(2)	2.444(3)	2.422(2)
	O(1) \times 4	2.776(1)	2.778(1)	2.763(1)
	O(2) \times 4	2.682(1)	2.657(1)	2.655(1)
Fe/Co	O(1) \times 2	2.016(1)	2.002(2)	2.078(1)
	O(2) \times 4	1.958(1)	1.959(1)	1.944(1)

Table 1. Selected bond lengths (Å) from the refined structures of $\text{Sr}_2\text{Fe}_{0.5}\text{Ir}_{0.5}\text{O}_4$, $\text{Sr}_2\text{Co}_{0.5}\text{Ir}_{0.5}\text{O}_4$ and $\text{La}_{0.5}\text{Sr}_{1.5}\text{Co}_{0.5}\text{Ir}_{0.5}\text{O}_4$.

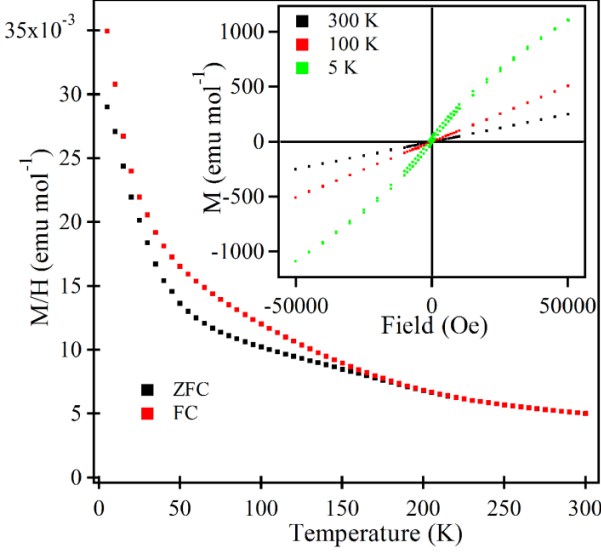


Figure 3. Zero-field cooled and field cooled magnetization data collected from $\text{Sr}_2\text{Fe}_{0.5}\text{Ir}_{0.5}\text{O}_4$ as a function of temperature in an applied field of 100 Oe. Inset shows magnetization-field isotherms at 5, 100 and 300 K.

through the origin, in contrast to analogous data collected at 5 K which shows a sigmoidal shape and hysteresis. The linear magnetization-field data at 100 K suggest that the small divergence between ZFC and FC data observed below 170 K comes from a small concentration of a secondary phase (not observable by diffraction) rather than the bulk sample, with the bulk sample undergoing magnetic order at $T \sim 50$ K. AC susceptibility data collected as a function of temperature from $\text{Sr}_2\text{Fe}_{0.5}\text{Ir}_{0.5}\text{O}_4$ (Figure S1, in the Supporting Information) follow the form of the ZFC data and show no frequency dependence, again consistent with the idea that the divergence at 170 K is due to an impurity phase.

To investigate any magnetic order present at low temperature in $\text{Sr}_2\text{Fe}_{0.5}\text{Ir}_{0.5}\text{O}_4$, neutron powder diffraction data were collected at 5 K (Figure 4). This data set exhibits a single weak, broad, asymmetric diffraction peak not observed in the analogous 300 K data, which can be indexed as the $[1, 0, 1]$ reflection of an $a' = \sqrt{2}a$, $b' = \sqrt{2}b$, $c' = c$ geometrically expanded unit cell. A single magnetic diffraction peak does not allow a magnetic model to be refined, however the simplest \mathbf{k} -vector compatible with this peak is $\mathbf{k} = (\frac{1}{2}, -\frac{1}{2}, 0)$ which suggests an antiferromagnetic state, with the weak, broad nature of the magnetic diffraction peak indicating the length-scale and size of the ordered moment is small.

Magnetic characterization of $\text{A}_2\text{Co}_{0.5}\text{Ir}_{0.5}\text{O}_4$. DC magnetization data collected from $\text{Sr}_2\text{Co}_{0.5}\text{Ir}_{0.5}\text{O}_4$ and $\text{La}_{0.5}\text{Sr}_{1.5}\text{Co}_{0.5}\text{Ir}_{0.5}\text{O}_4$ are shown in Figure 5 and 6 respectively. The ZFC and FC data from both samples diverge weakly below $T \sim 150$ K with the ZFC data exhibiting a local maximum at 35 K and 15 K for $\text{Sr}_2\text{Co}_{0.5}\text{Ir}_{0.5}\text{O}_4$ and $\text{La}_{0.5}\text{Sr}_{1.5}\text{Co}_{0.5}\text{Ir}_{0.5}\text{O}_4$ respectively. Magnetization-field data collected from both samples at 300 K are linear and pass through

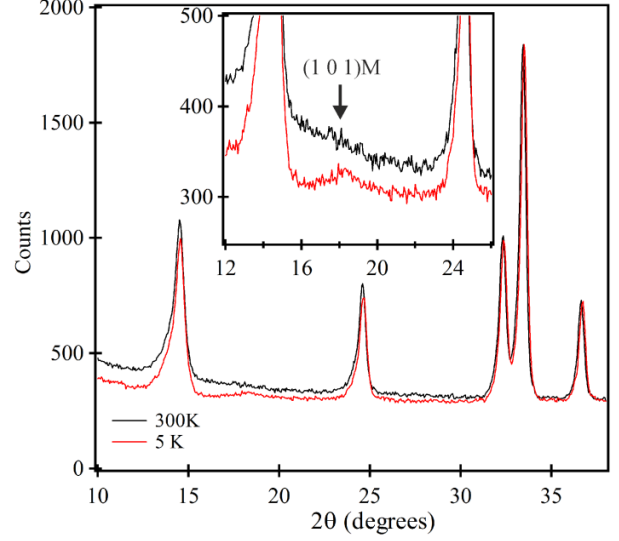


Figure 4. Comparison of neutron powder diffraction data collected from $\text{Sr}_2\text{Fe}_{0.5}\text{Ir}_{0.5}\text{O}_4$ at 300 K and 5 K. An additional feature in 5 K data set can be indexed as the $[1, 0, 1]$ reflection of $\sqrt{2} \times \sqrt{2} \times 1$ geometrically expanded unit cell.

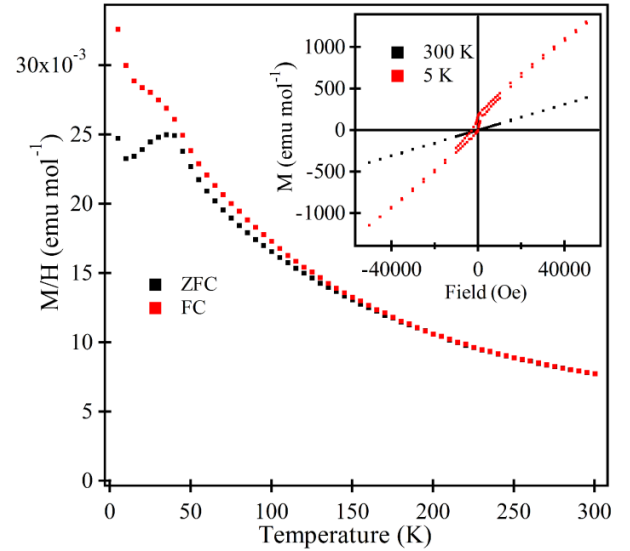


Figure 5. Zero-field cooled and field cooled magnetization data collected from $\text{Sr}_2\text{Co}_{0.5}\text{Ir}_{0.5}\text{O}_4$ as a function of temperature. Inset shows magnetization-field data collected after cooling from 300 K in a 50,000 Oe field.

the origin, however analogous data collected at 5 K after cooling in an applied field of 50 kOe (Figure 5 and Figure S2 in the supporting information) exhibit hysteresis and are offset from the

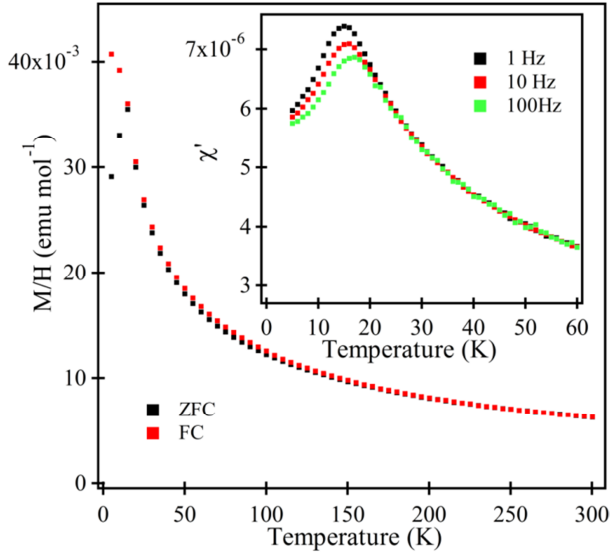


Figure 6. Zero-field cooled and field cooled magnetization data collected from $\text{La}_{0.5}\text{Sr}_{1.5}\text{Co}_{0.5}\text{Ir}_{0.5}\text{O}_4$ in an applied field of 100 Oe. Inset shows ac susceptibility as a function of temperature measured at 1, 10 and 100 Hz.

origin. AC susceptibility data collected from $\text{La}_{0.5}\text{Sr}_{1.5}\text{Co}_{0.5}\text{Ir}_{0.5}\text{O}_4$ (inset Figure 6) follow the form of the ZFC data, with the maximum at $T \sim 15$ K showing a strong frequency dependence. These data suggest that, in common with $\text{Sr}_2\text{Fe}_{0.5}\text{Ir}_{0.5}\text{O}_4$, the weak divergence between ZFC and FC data below $T \sim 150$ K is due to a secondary phase, with the lower temperature transitions in both cobalt phases being the freezing of spin-glass states. The magnetic behavior we observe for $\text{Sr}_2\text{Co}_{0.5}\text{Ir}_{0.5}\text{O}_4$ is in agreement with previous reports.¹² Neutron diffraction data collected from $\text{La}_{0.5}\text{Sr}_{1.5}\text{Ir}_{0.5}\text{O}_{4-x}$ at 5 K show no evidence for magnetic order. Analogous low-temperature neutron diffraction data have been collected from $\text{Sr}_2\text{Co}_{0.5}\text{Ir}_{0.5}\text{O}_4$ previously,¹² and these also show no evidence for magnetic order.

Chemical and structural characterization of $\text{A}_2\text{M}_{0.5}\text{Ir}_{0.5}\text{O}_3$ phases. Thermogravimetric data collected while heating the zirconium-reduced samples of $\text{Sr}_2\text{Fe}_{0.5}\text{Ir}_{0.5}\text{O}_{4-x}$, $\text{Sr}_2\text{Co}_{0.5}\text{Ir}_{0.5}\text{O}_{4-x}$ and $\text{La}_{0.5}\text{Sr}_{1.5}\text{Co}_{0.5}\text{Ir}_{0.5}\text{O}_{4-x}$ under flowing oxygen to recover the oxygen stoichiometric $\text{A}_2\text{M}_{0.5}\text{Ir}_{0.5}\text{O}_4$ phases (confirmed by powder X-ray diffraction) revealed mass gains of 3.73 %, 3.60 %, and 3.38 % respectively, corresponding to compositions of $\text{Sr}_2\text{Fe}_{0.5}\text{Ir}_{0.5}\text{O}_{3.08(2)}$, $\text{Sr}_2\text{Co}_{0.5}\text{Ir}_{0.5}\text{O}_{3.08(3)}$ and $\text{La}_{0.5}\text{Sr}_{1.5}\text{Co}_{0.5}\text{Ir}_{0.5}\text{O}_{2.98(3)}$ respectively when secondary phases are taken into consideration as described in detail in Figures S3, S4 and S5 in the Supporting Information. These phases will henceforth be referred to as $\text{Sr}_2\text{Fe}_{0.5}\text{Ir}_{0.5}\text{O}_3$, $\text{Sr}_2\text{Co}_{0.5}\text{Ir}_{0.5}\text{O}_3$ and $\text{La}_{0.5}\text{Sr}_{1.5}\text{Co}_{0.5}\text{Ir}_{0.5}\text{O}_3$.

Neutron powder diffraction data collected from $\text{Sr}_2\text{Fe}_{0.5}\text{Ir}_{0.5}\text{O}_3$, $\text{Sr}_2\text{Co}_{0.5}\text{Ir}_{0.5}\text{O}_3$ and $\text{La}_{0.5}\text{Sr}_{1.5}\text{Co}_{0.5}\text{Ir}_{0.5}\text{O}_3$ at 298 K could all be indexed on the basis of body-centered orthorhombic unit cells, suggesting the reduced phases adopt structures analogous to that of Sr_2FeO_3 .¹⁷ Structural models based on the structure of Sr_2FeO_3 were constructed with an appropriate Fe/Ir or Co/Ir solid solution on the B-site and a 1:3 La:Sr solid solution on the A-site of the $\text{La}_{0.5}\text{Sr}_{1.5}\text{Co}_{0.5}\text{Ir}_{0.5}\text{O}_3$ model. These models were refined against the neutron diffraction data. In all the refinements all atomic positional parameters were refined as were anisotropic atomic displacement parameters for all atoms. Close inspection of the data collected from all three samples revealed the presence of a SrO secondary phase, so this was added to the structural models. All three refinements converged readily to give good fits to the data.

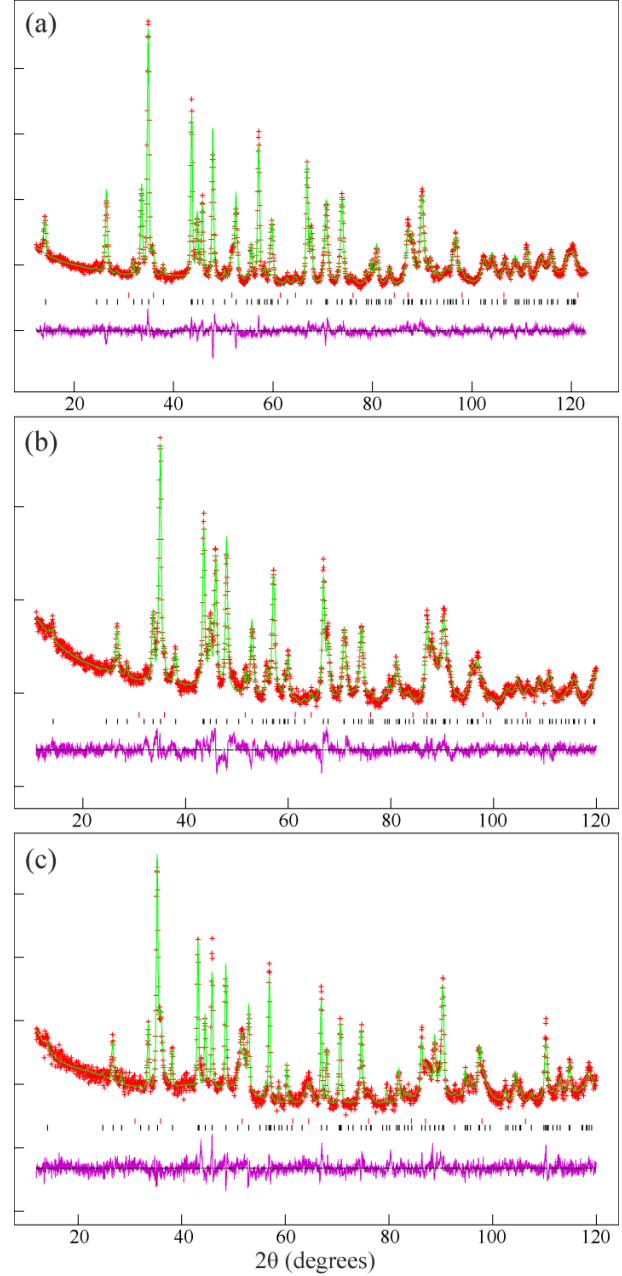


Figure 7. Observed, calculated and difference plots from the structural refinement of a) $\text{Sr}_2\text{Fe}_{0.5}\text{Ir}_{0.5}\text{O}_3$, b) $\text{Sr}_2\text{Co}_{0.5}\text{Ir}_{0.5}\text{O}_3$ and c) $\text{La}_{0.5}\text{Sr}_{1.5}\text{Co}_{0.5}\text{Ir}_{0.5}\text{O}_3$ against neutron powder diffraction data collected at 298 K. Lower tick marks indicate peak positions from the majority phase, upper tick marks for an SrO secondary phase. The unindexed peaks at $2\theta \sim 45^\circ$ come from the vanadium sample holder.

Full details of the refined structures of $\text{Sr}_2\text{Fe}_{0.5}\text{Ir}_{0.5}\text{O}_3$, $\text{Sr}_2\text{Co}_{0.5}\text{Ir}_{0.5}\text{O}_3$ and $\text{La}_{0.5}\text{Sr}_{1.5}\text{Co}_{0.5}\text{Ir}_{0.5}\text{O}_3$ are given in Tables S4, S5 and S6 respectively in the supporting information with plots of the observed and calculated data shown in Figures 7a, 7b and 7c respectively and selected bond lengths are listed in Table 2.

Magnetic characterization of $\text{Sr}_2\text{Fe}_{0.5}\text{Ir}_{0.5}\text{O}_3$. ZFC and FC DC magnetization data collected from $\text{Sr}_2\text{Fe}_{0.5}\text{Ir}_{0.5}\text{O}_3$ as a function of temperature, in an applied field of 100 Oe, are shown in Figure 8. On cooling the ZFC and FC data diverge weakly below $T \sim 150$ K, before the ZFC data goes through a maximum at 30 K consistent with a magnetic phase transition. The zero-field cooled

Cation	Anion	$\text{Sr}_2\text{Fe}_{0.5}\text{Ir}_{0.5}\text{O}_4$	$\text{Sr}_2\text{Co}_{0.5}\text{Ir}_{0.5}\text{O}_4$	$\text{La}_{0.5}\text{Sr}_{1.5}\text{Co}_{0.5}\text{Ir}_{0.5}\text{O}_4$
Sr/La	O(1) \times 1	2.471(3)	2.482(3)	2.468(7)
	O(1) \times 4	2.660(1)	2.658(1)	2.650(1)
	O(2) \times 2	2.626(1)	2.603(2)	2.607(3)
Fe/Co	O(1) \times 2	2.044(3)	2.066(1)	2.140(5)
	O(2) \times 2	1.963(1)	1.959(1)	1.940(1)

Table 2. Selected bond lengths (Å) from the refined structures of $\text{Sr}_2\text{Fe}_{0.5}\text{Ir}_{0.5}\text{O}_3$, $\text{Sr}_2\text{Co}_{0.5}\text{Ir}_{0.5}\text{O}_3$ and $\text{La}_{0.5}\text{Sr}_{1.5}\text{Co}_{0.5}\text{Ir}_{0.5}\text{O}_3$.

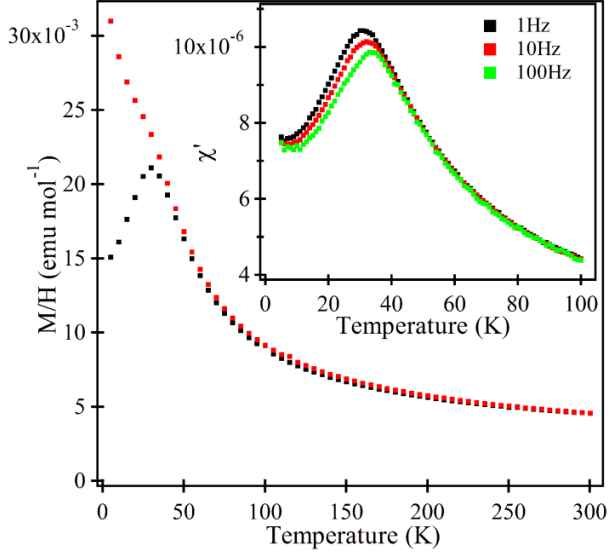


Figure 8. Zero-field cooled and field cooled magnetization data collected from $\text{Sr}_2\text{Fe}_{0.5}\text{Ir}_{0.5}\text{O}_3$ in an applied field of 100 Oe. Inset shows ac susceptibility as a function of temperature measured at 1, 10 and 100 Hz.

magnetization data can be fit by the Curie-Weiss law ($\chi = C/(T-\theta) + K$) in the temperature range $50 < T/K < 300$, to yield values of $C = 0.579(2) \text{ cm}^3 \text{ K mol}^{-1}$; $\theta = +8.5(2) \text{ K}$; $K = 0.0025(1) \text{ cm}^3 \text{ mol}^{-1}$. This value of the Curie constant is much smaller than expected for an $S = 2 \text{ Fe}^{2+}$ and $S = 1/2 \text{ Ir}^{2+}$ cation combination ($C_{\text{calc}} = 1.68 \text{ cm}^3 \text{ K mol}^{-1}$) which when considered in combination with the large temperature-independent contribution to the susceptibility, suggests the system is not a simple paramagnet, and that strong couplings exist between the local spins.

AC susceptibility data collected from $\text{Sr}_2\text{Fe}_{0.5}\text{Ir}_{0.5}\text{O}_3$ as a function of temperature at 1, 10 and 100 Hz (inset Figure 8) show the same local maximum as seen in the DC ZFC data, however the position of the maximum moves to higher temperature as the measuring frequency increases, indicating that this is a freezing transition of a spin-glass.

Magnetic characterization of $\text{A}_2\text{Co}_{0.5}\text{Ir}_{0.5}\text{O}_3$ phases. Magnetization data collected from $\text{Sr}_2\text{Co}_{0.5}\text{Ir}_{0.5}\text{O}_3$ and $\text{La}_{0.5}\text{Sr}_{1.5}\text{Co}_{0.5}\text{Ir}_{0.5}\text{O}_3$ indicate both samples are contaminated with a ferromagnetic impurity phase, presumably elemental cobalt. In order to extract the magnetic behavior of the majority phases, a ‘ferrosubtraction’ measurement technique was used. This approach exploits the observation that the susceptibility of a ferromagnet can be saturated in relatively small applied fields, allowing the magnetic behavior of the bulk phase to be measured, as explained in detail in the Supporting Information.

Figure 9 shows a plot of the paramagnetic susceptibility of $\text{Sr}_2\text{Co}_{0.5}\text{Ir}_{0.5}\text{O}_3$ as a function of temperature. These data can be fit by the Curie-Weiss law in the range $150 < T/K < 300$ to yield

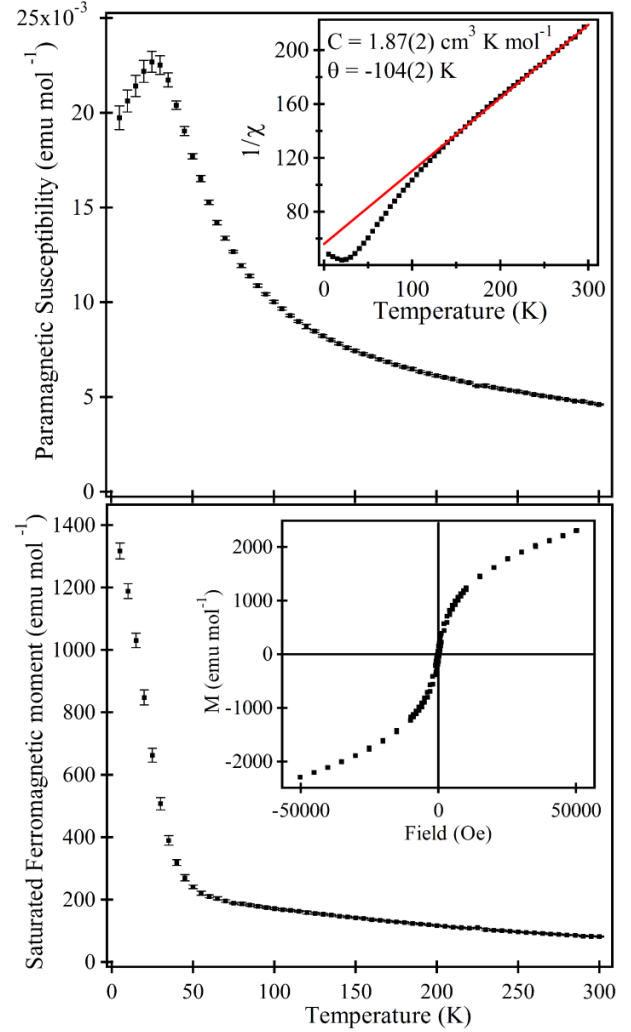


Figure 9. Paramagnetic susceptibility (top) and saturated ferromagnetic moment (bottom) of $\text{Sr}_2\text{Co}_{0.5}\text{Ir}_{0.5}\text{O}_3$. Inset to top panel shows fit to the Curie-Weiss law in the temperature range $150 < T/K < 300$. Inset to bottom panel shows magnetization-field data collected at 5 K after cooling in 50 KOe field from 300 K.

values of $C = 1.87(2) \text{ cm}^3 \text{ K mol}^{-1}$ and $\theta = -104 \text{ K}$. This value of the Curie constant is larger than expected for the combination of spin-only $S = 3/2$, Co^{2+} and $S = 1/2$, Ir^{2+} centres ($C_{\text{calc}} = 1.12 \text{ cm}^3 \text{ K mol}^{-1}$) indicating that there is a strong orbital contribution to the moment from either Co^{2+} or Ir^{2+} and/or strong spin-spin interactions in the system. On cooling below 150 K the paramagnetic susceptibility deviates from the Curie-Weiss law and goes through a maximum $T = 25 \text{ K}$. This is associated with a sharp increase in the saturated ferromagnetic moment of the system, suggesting the

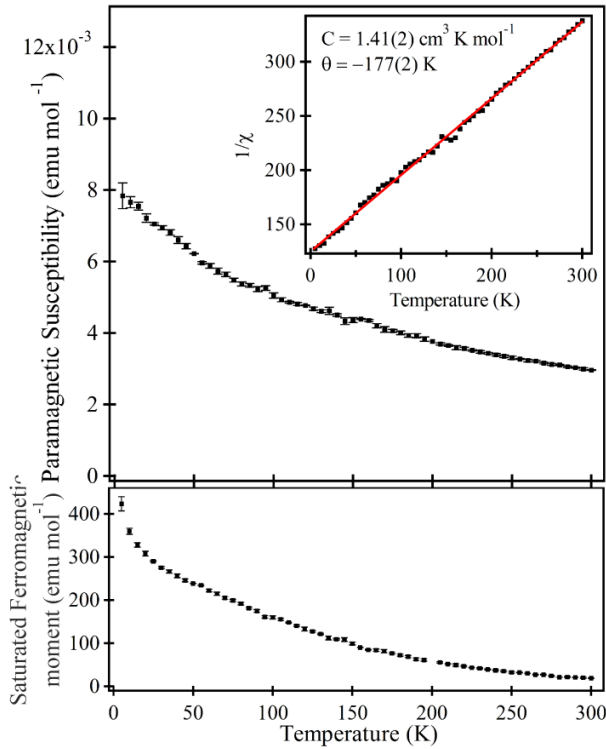


Figure 10. Paramagnetic susceptibility (top) and saturated ferromagnetic moment (bottom) of $\text{La}_{0.5}\text{Sr}_{1.5}\text{Co}_{0.5}\text{Ir}_{0.5}\text{O}_3$. Inset to top panel shows fit to the Curie-Weiss law in the temperature range $5 < T/K < 300$.

onset of canted antiferromagnetic order (weak ferromagnetism), however neutron powder diffraction data collected at 5 K show no indication of long-range magnetic order. Magnetization-field data collected from $\text{Sr}_2\text{Co}_{0.5}\text{Ir}_{0.5}\text{O}_3$ at 5 K, after cooling from 300 K in an applied field of 50 kOe, are centered on the origin (see inset to Figure 9) unlike data collected the $\text{Sr}_2\text{Co}_{0.5}\text{Ir}_{0.5}\text{O}_4$ ‘parent’ phase, suggesting that reduction has removed the frustrated magnetic couplings from the oxidized system.

Figure 10 shows the paramagnetic susceptibility and saturated ferromagnetic moment of $\text{La}_{0.5}\text{Sr}_{1.5}\text{Co}_{0.5}\text{Ir}_{0.5}\text{O}_4$ measured via the ferrosubtraction technique. Both data sets increase with decreasing temperature and show no sign of an ordering transition. The paramagnetic susceptibility can be fitted by the Curie-Weiss law over the range $5 < T/K < 300$ to yield values of $C = 1.41(2) \text{ cm}^3 \text{ K mol}^{-1}$ and $\theta = -177(2) \text{ K}$. The value of the Curie constant is much larger than expected for the combination of $S = 1, \text{Co}^{1+}$ and $S = 1/2, \text{Ir}^{2+}$ centers ($C_{\text{calc}} = 0.687 \text{ cm}^3 \text{ K mol}^{-1}$), again suggesting either a strong orbital component to the moment or strong spin-spin interactions, with further evidence for the latter interactions coming from the large value of the Weiss temperature.

Discussion

Neutron powder diffraction data collected from $\text{Sr}_2\text{Fe}_{0.5}\text{Ir}_{0.5}\text{O}_4$, $\text{Sr}_2\text{Co}_{0.5}\text{Ir}_{0.5}\text{O}_4$ and $\text{La}_{0.5}\text{Sr}_{1.5}\text{Co}_{0.5}\text{Ir}_{0.5}\text{O}_4$ show that all three phases adopt cation-disordered, $n = 1$ Ruddlesden-Popper structures with tetragonal $I4/mmm$ symmetry, and thus no indication of the cooperative tilting distortion observed from the IrO_6 units in Sr_2IrO_4 .¹⁸ Reduction of the $\text{A}_2\text{M}_{0.5}\text{Ir}_{0.5}\text{O}_4$ phases with a Zr getter converts them topochemically into the corresponding $\text{A}_2\text{M}_{0.5}\text{Ir}_{0.5}\text{O}_3$ phases, $\text{Sr}_2\text{Fe}_{0.5}\text{Ir}_{0.5}\text{O}_3$, $\text{Sr}_2\text{Co}_{0.5}\text{Ir}_{0.5}\text{O}_3$ and $\text{La}_{0.5}\text{Sr}_{1.5}\text{Co}_{0.5}\text{Ir}_{0.5}\text{O}_3$, in which the transition-metal cations are located in approximately square-planar coordination sites which are linked into 1-dimensional chains, as shown in Figure 11.

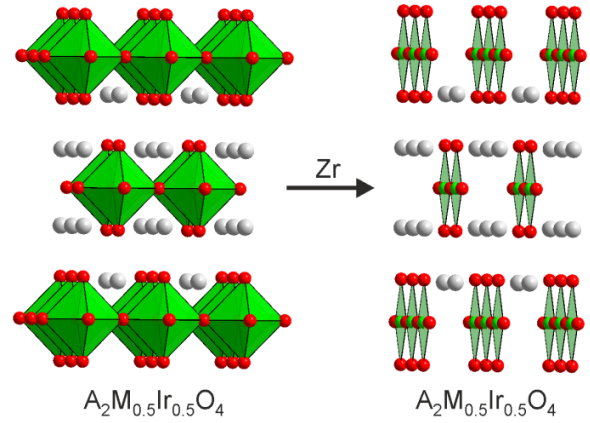


Figure 11. A schematic diagram show the change in structure on conversion of $\text{A}_2\text{M}_{0.5}\text{Ir}_{0.5}\text{O}_4$ $n = 1$ Ruddlesden-Popper phases to $\text{A}_2\text{M}_{0.5}\text{Ir}_{0.5}\text{O}_3$ phases. Gray, red and green sphere represent A, O and M/Ir respectively.

Transition-metal oxidation states in $\text{A}_2\text{M}_{0.5}\text{Ir}_{0.5}\text{O}_4$ and $\text{A}_2\text{M}_{0.5}\text{Ir}_{0.5}\text{O}_3$ phases. The oxidation states of the transition-metal cations in the $\text{Sr}_2\text{Fe}_{0.5}\text{Ir}_{0.5}\text{O}_4$, $\text{Sr}_2\text{Co}_{0.5}\text{Ir}_{0.5}\text{O}_4$ and $\text{La}_{0.5}\text{Sr}_{1.5}\text{Co}_{0.5}\text{Ir}_{0.5}\text{O}_4$ are in principle ambiguous, however the analogous double perovskite phases $\text{Sr}_2\text{FeIrO}_6$, $\text{Sr}_2\text{CoIrO}_6$ and LaSrCoIrO_6 are all adopt an Ir^{5+} oxidation state, as confirmed by experimental and computational studies, with the other transition-metal being Fe^{3+} , Co^{3+} and Co^{2+} respectively.¹⁹⁻²⁰ The transition-metal oxygen bond lengths in the $\text{A}_2\text{M}_{0.5}\text{Ir}_{0.5}\text{O}_4$ phases (Table 1) are consistent with these oxidation state combinations being retained in the Ruddlesden-Popper phases and in the case of $\text{Sr}_2\text{Fe}_{0.5}\text{Ir}_{0.5}\text{O}_4$ and $\text{Sr}_2\text{Co}_{0.5}\text{Ir}_{0.5}\text{O}_4$ these $\text{M}^{3+}/\text{Ir}^{5+}$ oxidation state assignments are supported by DFT calculations²¹ and XAS measurements in the case of $\text{Sr}_2\text{Co}_{0.5}\text{Ir}_{0.5}\text{O}_4$.¹²

Topochemical reduction of $\text{Sr}_2\text{Fe}_{0.5}\text{Ir}_{0.5}\text{O}_4$ to $\text{Sr}_2\text{Fe}_{0.5}\text{Ir}_{0.5}\text{O}_3$ is directly analogous to the reduction of the double perovskite $\text{Sr}_2\text{FeIrO}_6$ to $\text{Sr}_2\text{FeIrO}_4$ – there is the same change in average transition-metal oxidation state and the transition-metal cations reside in the square-planar coordination sites in both reduced phases. Thus we can anticipate that the $\text{Fe}^{2+}/\text{Ir}^{2+}$ oxidation state combination present in $\text{Sr}_2\text{FeIrO}_4$ is also present in $\text{Sr}_2\text{Fe}_{0.5}\text{Ir}_{0.5}\text{O}_3$ – an idea which is supported by noting that the average $\text{Ir}/\text{Fe}-\text{O}$ bond length of the $(\text{Fe}/\text{Ir})\text{O}_4$ coordination site of $\text{Sr}_2\text{Fe}_{0.5}\text{Ir}_{0.5}\text{O}_3$ (2.003 Å, Table 2) is almost identical to the average of the $\text{Fe}-\text{O}$ and $\text{Ir}-\text{O}$ bond lengths in $\text{Sr}_2\text{FeIrO}_4$ (1.996 Å).¹⁰

The analogous reductions of the cobalt double perovskite phases $\text{Sr}_2\text{CoIrO}_6$ and LaSrCoIrO_6 have not yet been achieved, despite multiple attempts, so the hypothetical reduced phases cannot provide guidance as to the oxidation state combinations present in $\text{Sr}_2\text{Co}_{0.5}\text{Ir}_{0.5}\text{O}_3$ and $\text{La}_{0.5}\text{Sr}_{1.5}\text{Co}_{0.5}\text{Ir}_{0.5}\text{O}_3$. However a comparison of the average $(\text{Co}/\text{Ir})-\text{O}$ bond length in $\text{Sr}_2\text{Co}_{0.5}\text{Ir}_{0.5}\text{O}_3$ (2.012 Å, Table 2) with the $\text{Ir}-\text{O}$ bond length in the Ir^{2+}O_4 units in $\text{Sr}_2\text{FeIrO}_6$ (1.982 Å)¹⁰ and the $\text{Co}-\text{O}$ bond length in the Co^{2+}O_4 units in $\text{Sr}_3\text{Co}_2\text{O}_4\text{Cl}_2$ (2.008 Å)²² indicate a $\text{Co}^{2+}/\text{Ir}^{2+}$ combination for $\text{Sr}_2\text{Co}_{0.5}\text{Ir}_{0.5}\text{O}_3$, with a $\text{Co}^{1+}/\text{Ir}^{2+}$ combination being deduced for $\text{La}_{0.5}\text{Sr}_{1.5}\text{Co}_{0.5}\text{Ir}_{0.5}\text{O}_3$ by a similar method.²³

Thus we can see that iridium adopts an Ir^{5+} state in all the $\text{A}_2\text{M}_{0.5}\text{Ir}_{0.5}\text{O}_4$ phases and an Ir^{2+} state in all the $\text{A}_2\text{M}_{0.5}\text{Ir}_{0.5}\text{O}_3$ phases. As a result $\text{Sr}_2\text{Fe}_{0.5}\text{Ir}_{0.5}\text{O}_4$, $\text{Sr}_2\text{Co}_{0.5}\text{Ir}_{0.5}\text{O}_4$ and $\text{La}_{0.5}\text{Sr}_{1.5}\text{Co}_{0.5}\text{Ir}_{0.5}\text{O}_4$ form a series in which $d^4 \text{Ir}^{5+}$ is paired with $d^5 \text{Fe}^{3+}$, $d^6 \text{Co}^{3+}$ and $d^7 \text{Co}^{2+}$ while $\text{Sr}_2\text{Fe}_{0.5}\text{Ir}_{0.5}\text{O}_3$, $\text{Sr}_2\text{Co}_{0.5}\text{Ir}_{0.5}\text{O}_3$ and $\text{La}_{0.5}\text{Sr}_{1.5}\text{Co}_{0.5}\text{Ir}_{0.5}\text{O}_3$ form a series in which $d^7 \text{Ir}^{2+}$ is paired with $d^6 \text{Fe}^{2+}$, $d^7 \text{Co}^{2+}$ and $d^8 \text{Co}^{1+}$ allowing us to study the interaction magnetic couplings of these two series as a function of d-electron count.

Magnetic behavior. DC magnetization data collected from $\text{Sr}_2\text{Co}_{0.5}\text{Ir}_{0.5}\text{O}_4$ and $\text{La}_{0.5}\text{Sr}_{1.5}\text{Co}_{0.5}\text{Ir}_{0.5}\text{O}_4$ indicate both phases become spin glasses at low temperature, as confirmed by the frequency-dependent AC susceptibility measurements for $\text{La}_{0.5}\text{Sr}_{1.5}\text{Co}_{0.5}\text{Ir}_{0.5}\text{O}_4$ and previous measurements in the case of $\text{Sr}_2\text{Co}_{0.5}\text{Ir}_{0.5}\text{O}_4$.¹² This spin-glass behavior indicates that both Co/Ir phases exhibit a combination of crystallographic disorder (consistent with the diffraction data) and a frustration between the various Co-Co, Co-Ir and Ir-Ir magnetic couplings present.¹⁰

In contrast to the cobalt phases, $\text{Sr}_2\text{Fe}_{0.5}\text{Ir}_{0.5}\text{O}_4$ does not exhibit spin-glass behavior at low temperature and instead there is evidence for a short-range magnetically ordered state. Given that $\text{Sr}_2\text{Fe}_{0.5}\text{Ir}_{0.5}\text{O}_3$ (which shares a common cation lattice with $\text{Sr}_2\text{Fe}_{0.5}\text{Ir}_{0.5}\text{O}_4$) *does* exhibit spin-glass behavior we can conclude that both iron phases fulfil the crystallographic disorder criterion for spin-glass behavior, but in the case of $\text{Sr}_2\text{Fe}_{0.5}\text{Ir}_{0.5}\text{O}_4$ the Fe-Fe, Fe-Ir and Ir-Ir magnetic couplings are not frustrated.

As noted above the iridium centers adopt an Ir^{5+} oxidation state in the $\text{A}_2\text{M}_{0.5}\text{Ir}_{0.5}\text{O}_4$ phases. Strong spin-orbit coupling leads to Ir^{5+} adopting an essentially diamagnetic $J_{\text{eff}} = 0$ state so that magnetic couplings involving iridium can be neglected. We can therefore attribute the differing magnetic behavior of the iron and cobalt $\text{A}_2\text{M}_{0.5}\text{Ir}_{0.5}\text{O}_4$ phases to the d-electron counts of the 3d transition-metals. Fe^{3+} is d^5 and adopts an approximately spherically symmetric $S = 5/2$ electronic configuration so all the Fe-O-Fe superexchange couplings will be antiferromagnetic. In contrast Co^{3+} and Co^{2+} adopt asymmetric $S = 2$, $t_{2g}^4 e_g^2$ and $S = 3/2$, $t_{2g}^5 e_g^2$ configurations respectively which can yield antiferromagnetic or ferromagnetic π -superexchange interactions depending which orbitals interact, providing an origin for the magnetic frustration in these systems and thus rationalizing the observed behavior.

Magnetization data collected from all three $\text{A}_2\text{M}_{0.5}\text{Ir}_{0.5}\text{O}_3$ phases have a temperature dependence that can be fitted by the Curie-Weiss law, however the values of the Curie constant extracted from these fits do not correspond to those expected for simple spin-only, paramagnetic behavior of the constituent transition-metal cations, indicating strong spin-orbit and/or spin-spin interactions are present.

The structures of the $\text{A}_2\text{M}_{0.5}\text{Ir}_{0.5}\text{O}_3$ phases consist of approximately square-planar (M/Ir) O_4 coordination polyhedra connected *via* corner-sharing into chains, as shown in Figure 11. As a result, the magnetic interactions in these phases can be classified into three distinct types: i) intrachain (M/Ir)–O–(M/Ir) couplings, ii) in-plane interchain (M/Ir)–□–(M/Ir) couplings (where □ represents the location of an anion vacancy), and iii) interlayer couplings between the transition-metal cations in adjacent perovskite sheets.

Figure 12 shows the d-orbital fillings expected for Ir^{2+} , Fe^{2+} , Co^{2+} and Co^{1+} in square-planar coordination sites, by analogy to previously reported systems.^{10, 23–24} This shows that Fe^{2+} , Co^{2+} and Co^{1+} cations have a single electron in both the d_{xy} and $d_{x^2-y^2}$ orbital, while Ir^{2+} has only a single electron in d_{xy} with $d_{x^2-y^2}$ being empty. As a result we can expect strong intrachain couplings in all three $\text{A}_2\text{M}_{0.5}\text{Ir}_{0.5}\text{O}_3$ phases.

The interchain magnetic couplings in $\text{A}_2\text{M}_{0.5}\text{Ir}_{0.5}\text{O}_3$ phases will be mediated by electrons in the d_{z^2} , d_{xz} and d_{yz} orbitals. Figure 12 shows that Ir^{2+} , Fe^{2+} , Co^{2+} and Co^{1+} all have doubly occupied d_{z^2} orbitals, indicating that any interchain magnetic couplings in the $\text{A}_2\text{M}_{0.5}\text{Ir}_{0.5}\text{O}_3$ phases must be mediated through the d_{xz} or d_{yz} orbitals, as observed for the analogous interlayer couplings in the infinite layer phase SrFeO_2 .²⁴

As noted above Fe^{2+} , Co^{2+} and Co^{1+} form a series with increasing d-electron count which, as shown in Figure 12, successively fills the $d_{xz/yz}$ pseudo-degenerate pair of orbitals, so that $d^8 \text{Co}^{1+}$ has doubly occupied d_{xz} and d_{yz} orbitals. Given that Ir^{2+} also has

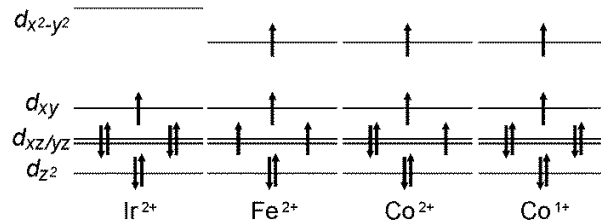


Figure 12. The local electronic configurations of Ir^{2+} , Fe^{2+} , Co^{2+} and Co^{1+} in MO_4 square-planar coordination environments.

doubly occupied d_{xz} and d_{yz} orbitals we would anticipate that $\text{La}_{0.5}\text{Sr}_{1.5}\text{Co}_{0.5}\text{Ir}_{0.5}\text{O}_3$ would have very weak interchain magnetic couplings, in agreement with the lack of a magnetic phase transition observed for this phase down to 5 K.

The $(d_{xz/yz})^2$ and $(d_{xz/yz})^3$ configurations of Fe^{2+} and Co^{2+} are expected to yield significant interchain magnetic couplings, and both $\text{Sr}_2\text{Fe}_{0.5}\text{Ir}_{0.5}\text{O}_3$ and $\text{Sr}_2\text{Co}_{0.5}\text{Ir}_{0.5}\text{O}_3$ exhibit magnetic phase transitions to a spin-glass state and an apparently canted antiferromagnetic state, respectively. The observation of spin-glass behavior for $\text{Sr}_2\text{Fe}_{0.5}\text{Ir}_{0.5}\text{O}_3$ is not surprising given the Fe/Ir cation disorder present in the phase and the complex competition between Fe-Ir and Ir-Ir couplings in the analogous reduced perovskite $\text{Sr}_2\text{FeIrO}_4$.¹⁰ What is perhaps a little surprising is that $\text{Sr}_2\text{Co}_{0.5}\text{Ir}_{0.5}\text{O}_3$ is not a spin-glass at low temperature, given that the couplings in $\text{Sr}_2\text{Fe}_{0.5}\text{Ir}_{0.5}\text{O}_3$ and $\text{Sr}_2\text{Co}_{0.5}\text{Ir}_{0.5}\text{O}_3$ are expected to be similar.

Conclusion

We have prepared a series of complex oxides in which first octahedrally coordinated $5d^4 \text{Ir}^{5+}$ cations are combined with $3d^5 \text{Fe}^{3+}$, $3d^6 \text{Co}^{3+}$ and $3d^7 \text{Co}^{2+}$ centers and then square-planar $5d^7 \text{Ir}^{2+}$ cations are combined with $3d^6 \text{Fe}^{2+}$, $3d^7 \text{Co}^{2+}$ and $3d^8 \text{Co}^{1+}$ centers. The collective magnetic behavior of these phases is dominated by the cation disorder between the iridium and 3d transition-metal cations which exist in these materials, resulting in three of the six phases exhibiting spin-glass behavior at low temperature. As a result it is hard to draw any definitive conclusions concerning the electronic analogy between octahedral Ir^{4+} and square-planar Ir^{2+} , however we do observe that none of the Ir^{2+} -containing phases have magnetic susceptibilities close to the spin-only values, suggesting strong orbital components to the local magnetic behavior.

ASSOCIATED CONTENT

Supporting Information

Structural parameters for $\text{Sr}_2\text{Fe}_{0.5}\text{Ir}_{0.5}\text{O}_4$, $\text{Sr}_2\text{Co}_{0.5}\text{Ir}_{0.5}\text{O}_4$, $\text{La}_{0.5}\text{Sr}_{1.5}\text{Co}_{0.5}\text{Ir}_{0.5}\text{O}_4$, $\text{Sr}_2\text{Fe}_{0.5}\text{Ir}_{0.5}\text{O}_3$, $\text{Sr}_2\text{Co}_{0.5}\text{Ir}_{0.5}\text{O}_3$ and $\text{La}_{0.5}\text{Sr}_{1.5}\text{Co}_{0.5}\text{Ir}_{0.5}\text{O}_3$ from refinement against neutron powder diffraction data at 298K; AC susceptibility of $\text{Sr}_2\text{Fe}_{0.5}\text{Ir}_{0.5}\text{O}_4$; Magnetization-field data from $\text{La}_{0.5}\text{Sr}_{1.5}\text{Co}_{0.5}\text{Ir}_{0.5}\text{O}_4$; Thermogravimetric analysis of $\text{Sr}_2\text{Fe}_{0.5}\text{Ir}_{0.5}\text{O}_3$, $\text{Sr}_2\text{Co}_{0.5}\text{Ir}_{0.5}\text{O}_3$ and $\text{La}_{0.5}\text{Sr}_{1.5}\text{Co}_{0.5}\text{Ir}_{0.5}\text{O}_3$; Description of magnetization measurements performed on samples containing ferromagnetic impurities.

AUTHOR INFORMATION

Corresponding Author

* michael.hayward@chem.ox.ac.uk

Author Contributions

The manuscript was written through contributions of all authors. The authors declare no competing financial interests.

ACKNOWLEDGMENT

We thank E. Suard for assistance collecting the neutron powder diffraction data. We thank The Leverhulme Trust grant award RPG-2014-366 “Topochemical reduction of 4d and 5d transition metal oxides” for supporting this work.

REFERENCES

1. Cao, G.; DeLong, L., *Frontiers of 4d- and 5d- Transition Metal Oxides*, 2013; p 1-319.
2. Cao, G.; Qi, T. F.; Li, L.; Terzic, J.; Yuan, S. J.; DeLong, L. E.; Murthy, G.; Kaul, R. K., Novel Magnetism of $\text{Ir}^{5+}(\text{5d}^4)$ ions in the Double Perovskite Sr_2YIrO_6 . *Phys. Rev. Lett.* **2014**, *112*, 056402.
3. Corredor, L. T.; Aslan-Cansever, G.; Sturza, M.; Manna, K.; Maljuk, A.; Gass, S.; Dey, T.; Wolter, A. U. B.; Kataeva, O.; Zimmermann, A.; Geyer, M.; Blum, C. G. F.; Wurmehl, S.; Buchner, B., Iridium double perovskite Sr_2YIrO_6 : A combined structural and specific heat study. *Phys. Rev. B* **2017**, *95*, 064418.
4. Terzic, J.; Zheng, H.; Ye, F.; Zhao, H. D.; Schlottmann, P.; De Long, L. E.; Yuan, S. J.; Cao, G., Evidence for a low-temperature magnetic ground state in double-perovskite iridates with $\text{Ir}^{5+}(\text{5d}^4)$ ions. *Phys. Rev. B* **2017**, *96*, 064436.
5. Page, J. E.; Topping, C. V.; Scrimshire, A.; Bingham, P. A.; Blundell, S. J.; Hayward, M. A., Doped $\text{Sr}_2\text{FeIrO}_6$ – phase separation and a $J_{\text{eff}} \neq 0$ state for Ir^{5+} . *Inorg. Chem.* **2018**, *57*, 10303-10311.
6. Jackeli, G.; Khaliullin, G., Mott Insulators in the Strong Spin-Orbit Coupling Limit: From Heisenberg to a Quantum Compass and Kitaev Models. *Phys. Rev. Lett.* **2009**, *102*.
7. Wang, F.; Senthil, T., Twisted Hubbard Model for Sr_2IrO_4 : Magnetism and Possible High Temperature Superconductivity. *Phys. Rev. Lett.* **2011**, *106*, 136402.
8. Yang, K. Y.; Lu, Y. M.; Ran, Y., Quantum Hall effects in a Weyl semimetal: Possible application in pyrochlore iridates. *Phys. Rev. B* **2011**, *84*, 075129.
9. Cao, G.; Bolivar, J.; McCall, S.; Crow, J. E.; Guertin, R. P., Weak ferromagnetism, metal-to-nonmetal transition, and negative differential resistivity in single-crystal Sr_2IrO_4 . *Phys. Rev. B* **1998**, *57*, R11039-R11042.
10. Page, J. E.; Morgan, H. W. T.; Zeng, D.; Manuel, P.; McGrady, J. E.; Hayward, M. A., $\text{Sr}_2\text{FeIrO}_4$: square-planar Ir(II) in an extended oxide. *Inorg. Chem.* **2018**, *57*, 13577-13585.
11. Kanungo, S.; Mogare, K.; Yan, B. H.; Reehuis, M.; Hoser, A.; Felser, C.; Jansen, M., Weak orbital ordering of Ir t_{2g} states in the double perovskite $\text{Sr}_2\text{CeIrO}_6$. *Phys. Rev. B* **2016**, *93*, 245148.
12. Mikhailova, D.; Hu, Z. W.; Kuo, C. Y.; Oswald, S.; Mogare, K. M.; Agrestini, S.; Lee, J. F.; Pao, C. W.; Chen, S. A.; Lee, J. M.; Haw, S. C.; Chen, J. M.; Liao, Y. F.; Ishii, H.; Tsuei, K. D.; Senyshyn, A.; Ehrenberg, H., Charge Transfer and Structural Anomaly in Stoichiometric Layered Perovskite $\text{Sr}_2\text{Co}_{0.5}\text{Ir}_{0.5}\text{O}_4$. *European Journal of Inorganic Chemistry* **2017**, 587-595.
13. Agrestini, S.; Kuo, C. Y.; Chen, K.; Utsumi, Y.; Mikhailova, D.; Rogalev, A.; Wilhelm, F.; Forster, T.; Matsumoto, A.; Takayama, T.; Takagi, H.; Haverkort, M. W.; Hu, Z.; Tjeng, L. H., Probing the $J(\text{eff})=0$ ground state and the Van Vleck paramagnetism of the Ir^{5+} ions in layered $\text{Sr}_2\text{Co}_{0.5}\text{Ir}_{0.5}\text{O}_4$. *Phys. Rev. B* **2018**, *97*, 214436.
14. Agrestini, S.; Kuo, C. Y.; Mikhailova, D.; Chen, K.; Ohresser, P.; Pi, T. W.; Guo, H.; Komarek, A. C.; Tanaka, A.; Hu, Z.; Tjeng, L. H., Intricacies of the Co^{3+} spin state in $\text{Sr}_2\text{Co}_{0.5}\text{Ir}_{0.5}\text{O}_4$: An x-ray absorption and magnetic circular dichroism study. *Phys. Rev. B* **2017**, *95*, 245131.
15. Gatimu, A. J.; Berthelot, R.; Muir, S.; Sleight, A. W.; Subramanian, M. A., Synthesis and characterization of $\text{Sr}_2\text{Ir}_{1-x}\text{M}_x\text{O}_4$ ($\text{M}=\text{Ti, Fe, Co}$) solid solutions. *J. Solid State Chem.* **2012**, *190*, 257-263.
16. Larson, A. C.; Von Dreele, R. B. *General Structure Analysis System*, Los Alamos National Laboratory Report LAUR 86-748: 2000.
17. Tassel, C.; Seiner, L.; Hayashi, N.; Ganesanpotti, S.; Ajiro, Y.; Kobayashi, Y.; Kageyama, H., Sr_2FeO_3 with Stacked Infinite Chains of FeO_4 Square Planes. *Inorg. Chem.* **2013**, *52*, 6096-6102.
18. Crawford, M. K.; Subramanian, M. A.; Harlow, R. L.; Fernandezbaca, J. A.; Wang, Z. R.; Johnston, D. C., Structural and Magnetic Studies of Sr_2IrO_4 . *Phys. Rev. B* **1994**, *49*, 9198-9201.
19. Battle, P. D.; Blake, G. R.; Gibb, T. C.; Vente, J. F., Structural chemistry and electronic properties of $\text{Sr}_2\text{FeIrO}_6$. *J. Solid State Chem.* **1999**, *145*, 541-548.
20. Narayanan, N.; Mikhailova, D.; Senyshyn, A.; Trots, D. M.; Laskowski, R.; Blaha, P.; Schwarz, K.; Fuess, H.; Ehrenberg, H., Temperature and composition dependence of crystal structures and magnetic and electronic properties of the double perovskites $\text{La}_{2-x}\text{Sr}_x\text{CoIrO}_6$ ($0 \leq x \leq 2$). *Phys. Rev. B* **2010**, *82*, 024403.
21. Ou, X. D.; Wu, H., Coupled charge-spin-orbital state in Fe- or Co-doped Sr_2IrO_4 . *Phys. Rev. B* **2014**, *89*, 035138.
22. Denis Romero, F.; Coyle, L.; Hayward, M. A., Structure and Magnetism of $\text{Sr}_3\text{Co}_2\text{O}_4\text{Cl}_2$ -An Electronically Driven Lattice Distortion in an Oxychloride Containing Square Planar Co-II Centers. *J. Am. Chem. Soc.* **2012**, *134*, 15946-15952.
23. Seddon, J.; Suard, E.; Hayward, M. A., Topotactic reduction of YBaCo_2O_5 and $\text{LaBaCo}_2\text{O}_5$: square-planar Co(I) in an extended oxide. *J. Am. Chem. Soc.* **2010**, *132*, 2802-2810.
24. Tsujimoto, Y.; Tassel, C.; Hayashi, N.; Watanabe, T.; Kageyama, H.; Yoshimura, K.; Takano, M.; Ceretti, M.; Ritter, C.; Paulus, W., Infinite-layer iron oxide with a square-planar coordination. *Nature* **2007**, *450*, 1062-1065.

For Table of Contents Only. Topochemical reduction of the $A_2M_{0.5}Ir^{5+}_{0.5}O_4$ phases $Sr_2Fe_{0.5}Ir_{0.5}O_4$, $Sr_2Co_{0.5}Ir_{0.5}O_4$ and $La_{0.5}Sr_{1.5}Co_{0.5}Ir_{0.5}O_4$ yields the $A_2M_{0.5}Ir^{2+}_{0.5}O_3$ phases $Sr_2Fe_{0.5}Ir_{0.5}O_3$, $Sr_2Co_{0.5}Ir_{0.5}O_3$ and $La_{0.5}Sr_{1.5}Co_{0.5}Ir_{0.5}O_3$ in which the Ir^{2+} and $Fe^{2+}/Co^{2+}/Co^{1+}$ cations are located in approximately square-planar coordination sites. The magnetic behavior of both the $A_2M_{0.5}Ir_{0.5}O_4$ and $A_2M_{0.5}Ir_{0.5}O_3$ phases can be rationalized on the basis of metal d-electron count and structural features.

